than in relation to the most probable binary mode concerned.

As originally stated, we have in this paper adopted a definition of corresponding modes in relation to binary and α-particle-accompanied ternary fission which imposed an initial bias towards a one-stage view of the ternary-fission process. On the naive assumption that calculated Q-value differences can be taken as indicative of the relative probabilities of occurrence of such corresponding modes, we have been led to the conclusion that the most favored ternary modes (when the fissioning nucleus is an even-even nucleus) are those in which the α particle accompanies two residual fragments each of which is an even-even species. The division

of mass and charge in binary fission being what it is, such ternary modes compete most favorably with the corresponding binary modes when the constituents of the α particle are taken exclusively from the nascent heavy fragment, subject to one general exception. The exception occurs when the binary mode is an odd-odd mode; then the ternary mode in which the two nascent fragments contribute equally to the emitted α particle is very highly favored indeed. In the light of these conclusions we merely reassert our former contention. Insofar as the constituents of the emitted α particle are contributed by a single fragment exclusively, then, formally at least, the process of ternary fission can be described equally well as a one- or two-stage process.

Excitation Functions, Recoil Ranges, and Statistical-Theory Analysis of Reactions Induced in Zr^{90} with 25- to 80-MeV Helium Ions*†

Yu-Wen Yu and Marshall Blann

Department of Chemistry and Nuclear Structure Research Laboratory,‡
University of Rochester, Rochester, New York

(Received 18 December 1967)

Excitation functions and mean recoil ranges have been measured for radioactive products resulting from the helium-ion bombardment of natural zirconium and targets which were isotopically enriched in Zr^{90}. Helium-ion energies varied between 25 and 80 MeV. Products observed were Mo^{90}, Nb^{90}, Zr^{89}, Zr^{88}, Y^{88}, Zr^{87}, Y^{87}, Zr^{86}, and Y^{86}. The excitation function was also measured for the production of Y^{87}. The recoil ranges are compared with the range theory of Lindhard, Scharff, and Schiott to determine the energy ranges over which the production of the nuclide is consistent with major contributions from a compound-nucleus mechanism. Excitation functions for products with $A \geq 87$ were compared with the statistical model to investigate the influence of shell structure on level densities. The level-density models used were those due to Newton and to Rosenzweig in addition to the standard Fermi-gas level density. Rosenzweig's model gave the best over-all agreement with the experimental results, with the standard Fermi-gas level density a close second. Several excitation functions were calculated using the s-wave approximation to estimate the effect of γ-ray de-excitation due to angular-momentum restrictions. Threshold position and excitation-function widths were found to agree quite satisfactorily with experimental values when this was done.

I. INTRODUCTION

THIS work was undertaken as part of a general survey of helium-ion-induced reactions, in particular, with targets near nuclear shell closures. Several conclusions[1] were reached from previous reaction studies around the $A = 60$ mass region: First, a major portion of the reaction cross sections could be attributed to a compound-nucleus mechanism up to excitations of 70 MeV (the upper limit of experimental measurements). Second, the statistical theory was quite adequate in reproducing the experimental energy variation of the various excitation functions measured if consideration was given to the influence of angular momentum on

γ-ray de-excitation.[2-10] Third, it was found that the correct magnitudes of the experimental excitation functions were calculated if Rosenzweig's shell-dependent level-density model[11] was used where the product nuclides were centered about the $N = Z = 28$ nucleon closed shell. Finally, it was found that, with the considerations referred to above for γ-ray de-excitation and level densities, there was no need for adjustment of other parameters, e.g., the level-spacing parameter was consistent with that predicted by a Fermi-gas model.[10]

[1] M. Blann, Nucl. Phys. 80, 223 (1966).

[2] D. Sperber, Phys. Rev. 138, B1024 (1965); 138, B1028 (1965).

[3] D. Sperber, Phys. Rev. 142, 478 (1966).

[4] J. R. Grover, Phys. Rev. 127, 2142 (1962).

[5] J. R. Grover, Phys. Rev. 123, 267 (1961).

[6] T. D. Thomas, Nucl. Phys. 53, 558 (1964); 53, 577 (1964).

[7] D. C. Williams and T. D. Thomas, Nucl. Phys. A92, 1 (1967).

[8] D. G. Sarantites and B. D. Pate, Nucl. Phys. A93, 545 (1967).

[9] J. R. Grover and J. Gilat, Phys. Rev. 157, 802 (1967); 157, 814 (1967); 157, 823 (1967).

[10] M. Blann, Phys. Rev. 157, 860 (1967).

[11] N. Rosenzweig, Phys. Rev. 105, 950 (1957); 108, 817 (1957).

In undertaking this investigation and similar studies with V^{51} and Au^{197} targets, the goal was to see if the apparent conclusions of the $A=60$ mass region could be generalized. A recent survey of (α,p) reactions by Swenson and Gruhn[12] indicates level-spacing parameters which are inconsistent with a Fermi-gas model. The question may be raised as to whether the (α,p) reaction is, because of the Coulomb effects, selecting direct reactions for observation in higher-Z targets, or whether the statistical assumption itself is invalid, and a more realistic nonequilibrium statistical model is required, e.g., as put forth by Griffin.[13]

In this paper, we present excitation functions and mean recoil ranges for a number of He^4 induced reactions of Zr^{90}. The recoil ranges will be used in conjunction with the range theory of Lindhard et al.[14] to determine (within the limits allowed by recoil range data) the energy regions in which individual excitation functions are consistent with a reaction proceeding predominantly with full momentum transfer followed by particle emission which is symmetric about 90° c.m. We next will analyze these data with the statistical theory using different shell-dependent level densities, in an attempt to see if either of the models used is clearly superior to the others, as was the case in the Ni^{56} region.[1] We will also apply the s-wave approximation to a few representative excitation functions to see if the positions on the energy axis and widths are consistent with the predictions of the statistical theory, when allowance is made for a γ-ray cascade following particle emission.[2–10,15]

II. EXPERIMENTAL PROCEDURES

A. Targets and Bombardments

Both natural and enriched zirconium foils were used in this work. The natural Zr foils were 0.5 mil thick with an estimated uniformity of $\pm3\%$ (8.3 ± 0.3 mg/cm²). Purity was 99.97%. Some of the targets (97.8% enriched in Zr^{90}) were 2–5 mg/cm² foils, and some were prepared by evaporation of Zr^{90} onto 0.5-mil, 99.99% pure aluminum foil. The thicknesses of evaporated Zr^{90} targets were determined from the weights of the aluminum foils before and after evaporation; thicknesses varied between 0.9 and 1 mg/cm².

Foil stacks were prepared with 99.99% pure, 0.5-mil (3.0 ± 0.5 mg/cm²) aluminum catcher foils, downstream from each Zr target. Five target stacks contained 12 such target-catcher pairs, one target stack contained 22.

Two bombardments were run on the Argonne National Laboratory 60-in. cyclotron, and four bombardments were made on the variable-energy Oak Ridge National Laboratory Isochronous Cyclotron (ORIC); pertinent data of each bombardment are summarized in Table I. The beam energies at ANL were determined by the range in aluminum foil, and those at ORIC were estimated from extraction radius and cyclotron frequency. The total beam exposures were obtained from current charts and from charge-integrator readings. The beams were all collimated to diameters less than the 1.9-cm target diameter.

B. Chemistry

Targets and their respective catcher foils were dissolved separately in 5 ml of $1N$ HF solution containing 10 mg each of Nb and Mo hold-back carriers (5 mg of Zr carrier was added to the solution containing the catcher foil). Then 5-mg Y carrier was added to the solution to precipitate YF_3.

After washing, the YF_3 precipitate was dissolved in $6N$ HCl, heated to dryness, then redissolved in $0.5N$ HCl; and finally Y was precipitated as the oxalate. The precipitates were washed with ethanol and ether, and dried in a desiccator under vacuum. Yields were determined gravimetrically.

The Zr was precipitated from the supernate by $Ba(NO_3)_2$ as $BaZrF_6$ and dissolved in 10-ml H_3BO_3 +HCl solution. Ba^{++} was precipitated by H_2SO_4; the supernate was diluted to 20 ml with water; and Zr was precipitated at 0°C with 5 ml of 6% cupferon solution (in 2 determinations) or 5 ml of 6% phenyl-arsonic-acid solution (in 4 determinations). The precipitates and filter papers were ignited at 800°C for an hour in porcelain crucibles to convert the precipitates to ZrO_2. The yields were determined gravimetrically.

TABLE I. Experimental details regarding the bombardments and targets.

Accelerator used	Target composition	Maximum beam energy (MeV)	Integrated charge (μA h)	Chemical separation
Argonne National Laboratory 60-in. cyclotron	Natural Zr foil	41.5	1.0	All foils
Argonne National Laboratory 60-in. cyclotron	Natural Zr foil	42.5	3.0	All foils
Oak Ridge National Laboratory isochronous cyclotron (ORIC)	Natural Zr foil	80	2.0	Odd targets and catcher foils
Oak Ridge National Laboratory isochronous cyclotron (ORIC)	Natural Zr foil	80	0.31	Even targets and catcher foils
Oak Ridge National Laboratory isochronous cyclotron (ORIC)	Enriched Zr^{90}	80	0.28	None
Oak Ridge National Laboratory isochronous cyclotron (ORIC)	Natural Zr foil	62	0.31	Even targets and catcher foils

[12] L. W. Swenson and C. R. Gruhn, Phys. Rev. **146**, 886 (1966).
[13] J. J. Griffin, Phys. Rev. Letters **17**, 478 (1966).
[14] J. Lindhard, M. Scharff, and H. E. Schiott, Kgl. Danske Videnskab. Selskab, Mat. Fys. Medd. **33**, No. 14 (1963).
[15] R. A. Esterlund and B. D. Pate, Nucl. Phys. **69**, 401 (1965).

C. Cross-Section and Recoil Range Determination

Table II summarizes the characteristics of radiation detected in the cross-section and recoil range determinations of this work. Positrons were counted with an end-window proportional counter which had been calibrated by the method of Bayhurst and Prestwood.[16] γ-scintillation spectrometry was performed with multichannel pulse-height analyzers with a 6-cc Ge(Li) detector and 3×3-in. NaI(Tl) crystals. The NaI(Tl) detector efficiencies were calculated from Heath's curves.[17] The Ge(Li) detector efficiency curves were determined from the counting rate of standard γ-ray sources which were standardized on a NaI(Tl) detector using Heath's curves.

The Bateman equations were applied where appro-priate to correct for genetic relationships in decay chains.[18,19] In the absolute counting-rate determinations, coincidence corrections were applied for all NaI(Tl) γ-ray measurements but were neglected in Ge(Li) γ-ray counting-rate calculations [since Ge(Li) detectors have very low counting efficiencies]. The over-all experimental errors of each measurement were estimated, based on the possible errors in chemical yields, target thickness, counting statistics, half-lives, counter efficiencies, integrator readings, and branching ratios. The estimated errors of cross sections and ranges of each reaction product measured are listed in the last two columns of Table II.

The cross sections and mean projected recoil ranges for reactions investigated in this work are listed in Tables III–VI. Results are shown graphically in Fig. 1.

TABLE II. Decay characteristics of isotopes studied in this work.

Nuclide	Type of radiation observed	Energy of radiation observed (MeV)	Assumed abundance (per decay)	Assumed half-life	Detection apparatus	Estimated errors (%) Cross sections	Recoil ranges
Mo⁹⁰	γ	0.122	0.85	5.7 hᵃ	Ge(Li)	±20	±10
Nb⁹⁰	γ	0.142	0.90	14.6 hᵇ	Ge(Li)	±20	±10
Zr⁸⁹	γ β⁺	0.915	1.00 0.25	79.3 hᶜ	NaI(Tl) and Ge(Li) end-window proportional counter	±20	±20
Zr⁸⁸	γ	0.39	1.00	85 dayᶜ	NaI(Tl)	±20	±15
Zr⁸⁷	γ	(Count 80 h Y⁸⁷ 0.48-MeV peak)	1.00	1.57 hᶜ	Ge(Li) and NaI(Tl)	±25	±20
Zr⁸⁶	γ	0.242	1.00	17 hᵈ	Ge(Li)	±20	±20
Y⁸⁸	γ	0.90	0.92	105 dayᵉ	NaI(Tl)	±20	±15
Y⁸⁷	γ	0.381 (Y⁸⁷ᵐ)	1.00	14 hᵉ			
		0.48 (Y⁸⁷ᵍ)	0.99	80 hᶜ	Ge(Li)	±30	
		0.389 (Sr⁸⁷)	1.00	2.8 hᶜ			
Y⁸⁶	γ	1.08	1.00	14.6 hᶠ	Ge(Li)	±20	±20

ᵃ John A. Cooper, thesis, University of California Radiation Laboratory Report No. UCRL-19610, 1966 (unpublished).
ᵇ J. A. Cooper, J. M. Hollander, M. I. Kalkstein, and J. O. Rasmussen, Nucl. Phys. 72, 113 (1965).
ᶜ Nuclear Data Sheets, compiled by K. Way et al. (U. S. Government Printing Office, National Academy of Sciences—National Research Council, Washington 25, D.C.), NRC [60–3–75], [60–3–85]; and N. G. Zaitseva, V. V. Kuznetsov, M. Ya Kuznetsova, Ma Ha Ik, G. Musiol, Han Shu-jun, Chou Mo-lung, and V. G. Chumin, Yadern. Fiz. 1, 385 (1965) [English transl: Soviet J. Nucl. Phys. 1, 273 (1965)].
ᵈ E. K. Hyde, W. J. Treytl, A. Siivola, D. H. Sisson, and D. K. Horen, Phys. Rev. 142, 657 (1966).
ᵉ M. Sakai, T. Yamazaki, and J. M. Hollander, Nucl. Phys. 84, 302 (1966).
ᶠ B. V. Nooijen, W. Lourens, H. V. Krugten, and A. H. Wapstra, Nucl. Phys. 63, 241 (1965).

TABLE III. Cross sections and ranges of reaction products produced by helium-ion bombardment of enriched Zr⁹⁰.

Helium-ion energyᵃ (MeV)	Target thickness T̄ (mg/cm²)	Mo⁹⁰ σ (mb)	R̄ (mg/cm²)	Nb⁹⁰ σ (mb)	R̄ (mg/cm²)	Zr⁸⁹ σ (mb)	R̄ (mg/cm²)	Zr⁸⁸ σ (mb)	R̄ (mg/cm²)	Y⁸⁸ σ (mb)	R̄ (mg/cm²)
79.5	0.93	46	0.43	227	0.38	338	0.55	69	0.35	30	0.38
77.5	1.03	51	0.41	205	0.44	291	0.51	60	0.34	25	0.38
75.5	0.97	50	0.45	215	0.47	297	0.45	48	0.38	24	0.38
73.5	1.17	60	0.47	250	0.44	285	0.41	46	0.30	27	0.40
71.5	0.95					220	0.40	47	0.35	26	0.33
69.5	0.90	86	0.43	311	0.42	166	0.34	58	0.34	32	0.39
67.5	0.95	77	0.44	278	0.46	205	0.38	70	0.24	28	0.46
65.5	4.72	87	0.47	333	0.45	141	0.27	62	0.37	22	0.46
63.0	4.08	89	0.36	329	0.50	117	0.21	72	0.40	24	0.46
60.5	5.08	88	0.45	311	0.40	85	0.17	79	0.43	20	0.47
57.5	4.31	77	0.40	298	0.46	64	0.19	87	0.39	21	0.41
54.5	1.99	35	0.38	149	0.39	31		75		21	0.39

ᵃ Energies based on range-energy values of C. F. Williamson, J. Boujot, and J. Picard, Saclay Report No. CEA-R3042, 1966 (unpublished).

[16] B. P. Bayhurst and R. J. Prestwood, Nucleonics 17, 82 (1959).
[17] R. L. Heath, Atomic Energy Commission Research and Development Report No. JD016408, 1957 (unpublished).
[18] H. Bateman, Proc. Cambridge Phil. Soc. 15, 423 (1910).
[19] G. Friedlander, J. W. Kennedy, and J. M. Miller, Nuclear and Radiochemistry (John Wiley & Sons, Inc., New York, 1964).

TABLE IV. Cross sections (mb) of reaction products produced by helium-ion bombardment of natural zirconium targets.

Helium-ion energy (MeV)	Mo90 [a]	Nb90 [a]	Zr89	Zr88 [b]	Zr87	Zr86	Y88 [b]	Y87	Y86
79.5	45	245		108			39		
78.1			423	92	99	17	47		
76.7	53	276	353	93		20	41	96	49
75.3			432	92	107	12	39	84	25
73.9	60	310	330	78		11	34		35
72.5			313	76	109	8.6	33	65	11
71.0	79	343	217	72		3.4	34		15
69.5			252	68	100	1.7	30	55	8.0
68.0	82	389	288	78		1.9	31		7.6
66.5			197	81	78		30	58	3.0
65.0	89	376	173	36			30		2.8
63.5			140	87	50		30	45	
62.0	80	327		86			36		
60.4			121	87	25		32	19	
58.8	46	257	86	86			29		
57.2			105	91	6.9		30	6.7	
55.5	22	177	80	79			26		
53.8			97	79			22		
52.0	49	71		63			22		
50.2				76			17		
48.2			71	49			16		
46.2			97	47			11		
44.2			75	20			8.8		
42.0			64	17			4.2		
41.0			61	15			3.0		
40.5			63	6.3			2.0		
39.5			57	7.6			1.6		
39.0			66	3.6			1.6		
38.0			61	4.1			0.87		
37.5			72	1.9					
36.5			63	1.5					
36.0			62						
35.0			50						
34.5			53						
33.5			50						
33.0			57						
32.0			32						
31.5			41						
30.5			33						
30.0			30						
29.0			20						
28.5			25						
27.5			9.3						

[a] No chemical separations were made.
[b] Average value of two bombardments.

The cross sections of each reaction were calculated from the sum of the activities in the target and catcher of a given nuclide. The mean projected recoil ranges were calculated from the following equation[20]:

$$\bar{R} = T[A_c/(A_c+A_T)][(\sigma_0+\sigma_T)/2\sigma_0], \quad (1)$$

where A_c and A_T are the activities of the product nuclide in the catcher foil and in the target foil, respectively. T is the target thickness, and σ_0 and σ_F are the cross sections at the front and back surfaces of the targets. If the energy loss of the helium ion in the target is sufficiently small $(\sigma_T=\sigma_0)$, then Eq. (1) will be reduced to

$$\bar{R} = T[A_c/(A_c+A_T)]. \quad (2)$$

[20] N. T. Porile, Phys. Rev. 135, A1115 (1964).

III. RESULTS AND DISCUSSION OF RECOIL RESULTS

A. Theoretical Range Relationship

In the last few years, there have been many recoil range studies tending to confirm the validity of the Lindhard, Scharff, and Schiott (LSS) range theory[14] over a fairly wide range of the energy and range variables used by LSS. Alexander[21] has summarized these measurements through 1966. It has also been shown that the LSS range theory agrees well with data in the specific region covered in this work (where some of the recoil ranges reported here were used for comparison with the LSS range predictions).[22]

[21] J. M. Alexander, in Nuclear Chemistry, edited by L. Yaffe (Academic Press Inc., New York, 1967).
[22] W. W. Bowman, F. M. Lanzafame, C. K. Cline, Y. Yu, and Marshall Blann, Phys. Rev. 165, 485 (1968).

Thus, a comparison between the ranges measured in this work and the predictions of LSS for compound-nucleus recoil products should indicate the region in which a given reaction results primarily from a compound-nucleus mechanism. In making such a comparison, it is essential that the LSS curve be corrected to the projected range and for the effects of particle evaporation from the recoils. The first correction is effected through use of curves provided by LSS; the second was accomplished by use of a computer program which calculates the proper projected range, given the average evaporation energies of up to five particles from a compound nucleus of specified kinetic energy. Each of the evaporated particles may have a different average kinetic energy, as for example in the case of an α particle and a neutron. Either an isotropic or a $1/\sin\theta$ angular distribution may be assumed, and the grid size for particle emission may be taken as low as $10°$, e.g., the range is computed by averaging over all ranges resulting from emission of particles at all permutations of $10°$ increments for each particle. As the number of particles out increases, time considerations require selection of a larger grid size. Since larger numbers of particles come out at higher excitations and, therefore, at higher recoil velocities, and since the change in range due to particle emission decreases with increasing recoil velocity, the larger grid size does not introduce any appreciable error ($\leq 2\%$). The choice of angular distribution ($1/\sin\theta$ or isotropic) does not significantly affect the range correction.

The LSS range curves, prior to correction for particle emission, are shown in Fig. 1 along with the corrected curves. Comparison of the two gives an idea of the

TABLE V. Recoil ranges of Zr isotopes produced by helium-ion bombardment of natural zirconium.

| Helium-ion energy (MeV) | Ranges in zirconium (mg/cm²) | | | |
Product:	Zr⁸⁹ [a]	Zr⁸⁸ [a]	Zr⁸⁷	Zr⁸⁶
78.1	0.53	0.54	0.81	0.72
75.3	0.54	0.52	0.56	0.56
72.5	0.50	0.46	0.62	0.51
69.5	0.46	0.55	0.52	
66.5	0.42	0.45	0.53	
63.5	0.37	0.48	0.52	
60.4	0.39	0.48		
57.2	0.31	0.42		
53.8	0.32	0.46		
50.2	0.30	0.43		
46.2	0.27	0.40		
42.0	0.36	0.38		
40.5	0.38			
39.0	0.28			
37.5	0.29			
36.0	0.35			
34.5	0.26			
33.0	0.30			
31.5	0.25			
30.0	0.31			
28.5	0.34			

[a] Average value of two bombardments.

TABLE VI. Recoil ranges of Mo⁹⁰, Nb⁹⁰, Y⁸⁸, and Y⁸⁶ produced by helium-ion bombardment of natural zirconium.

| Helium-ion energy (MeV) | Ranges in zirconium (mg/cm²) | | | |
Product:	Mo⁹⁰	Nb⁹⁰	Y⁸⁸ [a]	Y⁸⁶
79.5	0.69	0.60	0.56	
76.7	0.70	0.51	0.48	0.84
73.9	0.69	0.49	0.52	0.77
71.0			0.42	0.74
68.0	0.60	0.41	0.49	0.66
65.0	0.56	0.40	0.46	
62.0	0.42	0.43	0.43	
58.8	0.43	0.45	0.47	
55.5	0.41	0.39	0.49	
52.0	0.37	0.35	0.45	
48.2			0.47	
44.2			0.47	

[a] Average value of two bombardments.

sensitivity of ranges to the corrections described in this paragraph.

B. Ranges and Excitation Functions

Note that counting rates were too low to measure recoil ranges for Y⁸⁷. The shorthand reaction notation used in labeling the figures of this work implies that many reactions proceed via the emission of an α particle. While this is the case at lower excitation energies, the product yields at higher excitations must result primarily from evaporation of two neutrons and two protons rather than an α particle. The notation used in the figures is not intended to preclude the possibility of combinations of emitted particles other than α, but was used for simplicity of labeling.

Some general observations may be made with respect to the recoil ranges in Fig. 1(a)–1(g). First, up to the excitation function maxima, the ranges are consistent with a compound-nucleus mechanism. This statement must be tempered by the observation that, when only nucleons are emitted, the range will show a significant decrease only when there is a considerable contribution from low-momentum-transfer processes. Where an α particle is emitted, the range is considerably more sensitive to the reaction kinematics. Thus, in subsequent applications of the compound-nucleus model to these results, we are relying in many cases on the negative evidence that there is no evidence for large ($\gtrsim 30\%$) contributions of low-momentum-transfer reactions. The sensitivity of the range criterion to reactions involving incomplete momentum transfer has been discussed previously in greater detail.[23,24]

In the region past the excitation-function maxima, ranges from enriched Zr⁹⁰ targets show incomplete momentum transfer, while those resulting from natural targets are generally consistent with full momentum transfer. This implies an increasing contribution from direct interactions past the excitation-function maxima,

[23] J. P. Hazan and M. Blann, Phys. Rev. 137, B1202 (1965).
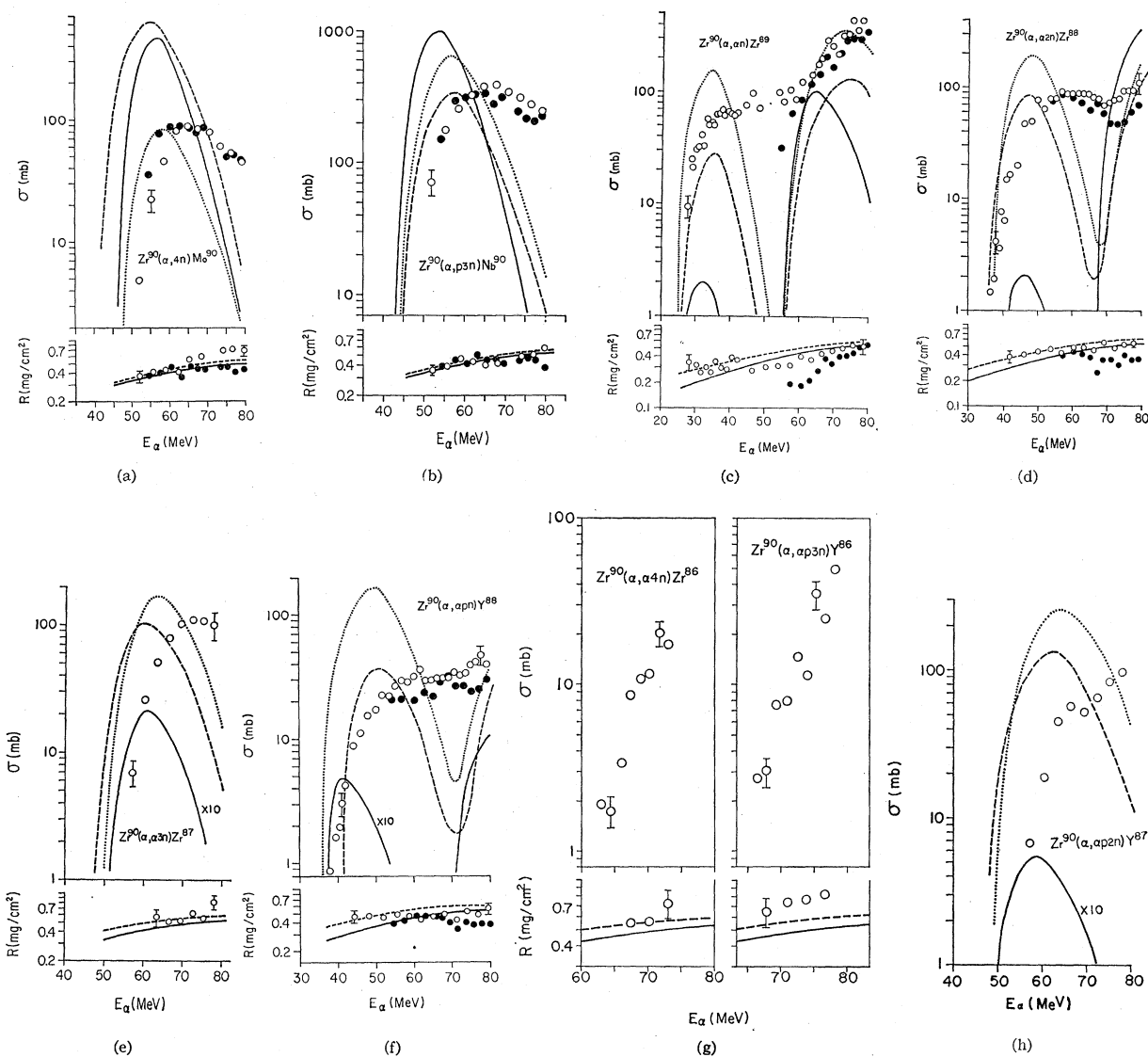[24] M. Blann and A. Ewart, Phys. Rev. 134, B783 (1964).

FIG. 1. The upper sets of points represent cross sections, the lower set the corresponding mean-recoil ranges. The abscissas are incident helium-ion kinetic energy. The closed circles represent measurements on enriched-Zr^{90} targets; open circles represent yields from natural-Zr targets (51% Zr^{90}, 11% Zr^{91}, 17% Zr^{92}, plus heavier isotopes). A few typical error flags are shown for cross sections and recoil ranges. The solid range curve is the LSS prediction for the projected ranges of the reaction products; the dashed curve is the LSS prediction corrected for the influence of particle emission as described in Sec. III A. The curves represent results of the statistical-theory calculations with the three level-density models described in the text. The dotted curves represent the standard Fermi-gas level-density results; the dashed curves represent Rosenzweig's model; and the solid curves represent Newton's model.

as has been observed previously.[24] The effect is not as noticeable with natural targets, since the ranges past the excitation-function maxima represent mainly the compound-nucleus contribution from Zr^{91} and Zr^{92}, where one is on the increasing side of the excitation functions. This observation is consistent with the difference in experimental cross sections between natural and enriched isotopes where the discrepancy in recoil ranges exists, and is also supported in the comparisons between calculated excitation functions in Zr^{90}, Zr^{91}, and Zr^{92} targets as indicated in Fig. 2.

For those reactions in which an α particle is emitted, the ranges from enriched targets often have a minimum followed by an increase with increasing bombarding energy. This is consistent with the cross section resulting from the α particle being inelastically scattered at the lower energy, with increasing contribution from a $2p$-$2n$-out compound-nucleus evaporation mechanism at the higher energies. This range behavior has also been observed[24] in helium-ion-induced reactions in Ni; the earlier work describes, in greater detail, the relationship between ranges and reaction kinematics.
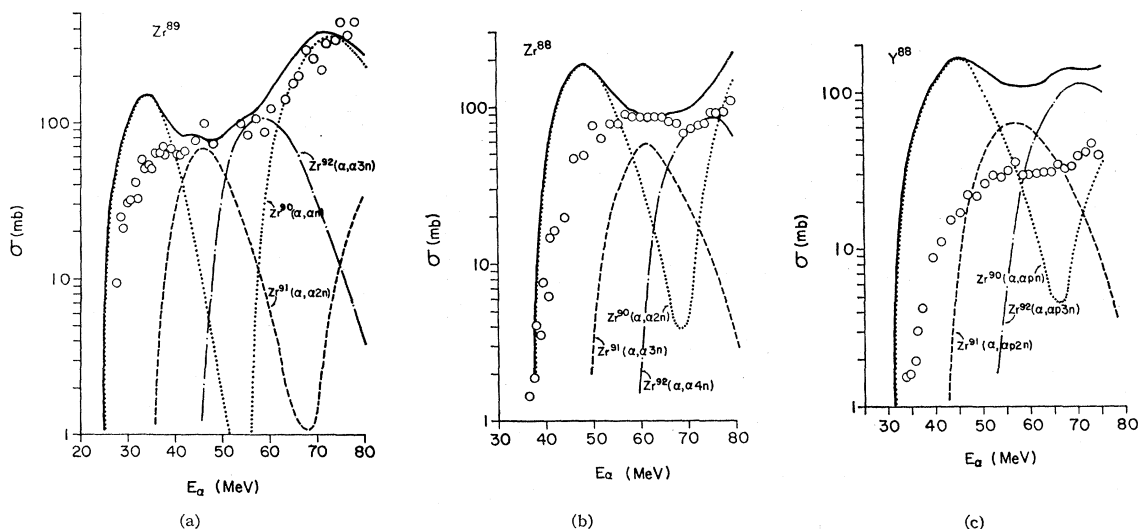
FIG. 2. Open points represent experimentally determined cross sections assuming yields result from Zr^{90} in natural-Zr foils. The dotted dashed, and dot-dash curves represent calculated values (standard level density) for contributions from Zr^{90}, Zr^{91}, and Zr^{92}, respectively, and have been adjusted for naturally occurring isotopic abundance. The solid curves are the sums of the calculated values for the three isotopes used in the calculations.

IV. STATISTICAL-THEORY ANALYSIS

In this section we outline the statistical-theory calculations used to interpret the excitation functions of Fig. 1. This will be done using three level-density models to assess the effect of the subshell closures on level densities. The models used will consist of a Fermi-gas level density (which will be referred to as a standard calculation),[25] one in which a shift in ground-state energy is introduced into the Fermi-gas expression according to Rosenzweig's model,[11] and one in which the Fermi-gas level-spacing parameter for each residual nuclide is a function of angular momentum of the last neutron and proton as suggested by Newton.[26] The discussion of level-density models is based on a discussion in an earlier publication.[1] Several excitation functions will be calculated using the s-wave approximation to see the upper limit of using a finite rather than infinite nuclear moment of inertia. Results of calculations in which the naturally occurring isotopic target composition has been used will be presented for several cases, to show the degree of usefulness of the statistical model in reproducing the experimental results.

A. Evaporation Calculations

The statistical theory as formulated by Weisskopf and Ewing[27] was used in the calculations of this work,

i.e.,

$$P_\nu(\epsilon)d\epsilon = \frac{(2s+1)_\nu \mu_\nu \epsilon \sigma_\nu(\epsilon)\rho(E_f)d\epsilon}{\sum_{\nu=1}^{n}(2s+1)_\nu \mu_\nu \int_0^\infty \epsilon \sigma_\nu(\epsilon)\rho(E_f)d\epsilon}, \quad (3)$$

where $P_\nu(\epsilon)d\epsilon$ (the probability of emitting the particle ν with channel energy between ϵ and $\epsilon+d\epsilon$) is related to the particle spin s, reduced mass μ, channel energy ϵ, inverse reaction cross section $\sigma_\nu(\epsilon)$, and residual-nucleus level density $\rho(E_f)$ as given in Eq. (3).

The computer programs used to evaluate Eq. (1) are described elsewhere.[1]

1. Inverse Reaction Cross Sections

Nonelastic cross sections calculated with the nuclear optical model were used for inverse reaction cross sections; neutron and proton cross sections were those reported by Mani et al[28]; α cross sections were those due to Igo and Huizenga.[29] Laboratory energies for α cross sections were converted graphically to channel energies before use. The α cross sections were also used for compound-nucleus cross sections, supplemented by extrapolated values for higher He^4 bombarding energies. Extrapolated values were subsequently checked against optical-model results with quite good agreement.

Many of the reaction products of this work arise from parent nuclides having proton binding energies

[25] T. Ericson, in *Advances in Physics*, edited by N. F. Mott (Taylor and Francis, Ltd., London, 1960), Vol. 9, p. 425.

[26] T. D. Newton, Can. J. Phys. **34**, 804 (1957).

[27] V. F. Weisskopf and D. H. Ewing, Phys. Rev. **57**, 472 (1940).

[28] G. S. Mani, I. Iori, and M. A. Melkanoff, Centre D'Etudes Nucléaires de Saclay Rapports C.E.A. No. 2379 and C.E.A. No. 2380, 1963 (unpublished).

[29] J. R. Huizenga and G. J. Igo, Argonne National Laboratory Report No. 6373, 1961 (unpublished). See also Nucl. Phys. **29**, 462 (1962).

which are considerably less than the neutron binding energies. Since the proton inverse cross sections go exponentially to zero at around 6 MeV kinetic energy, an arbitrary decision must be made concerning γ-ray-versus-proton-emission competition in the region of excitation below the proton Coulomb barrier and also below the neutron binding energy. The results to be summarized were made with two rather extreme assumptions concerning Γ_p/Γ_γ in this region. For one set of calculations, it was assumed that $\Gamma_p/\Gamma_\gamma=0$ in this region; in a second set, it was assumed that the γ-ray width was zero, i.e., any proton which thermodynamically could be emitted would be emitted. The calculated excitation functions presented in Figs. 1(a)–1(f), 1(h) are roughly in between these extremes, while the numbers used in the actual level-density analyses (last two figures) represent these extreme assumptions. Results of analysis of Zr^{86} and Y^{86} excitation functions are not shown for these level-density models, since the experimental results do not span a sufficient interval in energy for a meaningful analysis.

2. Nuclear Level Densities

As in previous calculations, a Fermi-gas level density was used for one set of calculations[25]:

$$\rho(E) \propto (E-\delta)^{-2} \exp(2[a(E-\delta)]^{1/2}), \qquad (4)$$

where it was assumed that

$$\rho(E,J) \propto (2J+1)\rho(E). \qquad (5)$$

These calculations will be referred to in the remainder of this work as "standard" calculations, i.e., the level density is a Fermi-gas level density, altered only for the odd-even (pairing) effect.

The energy gap δ was assumed to be equal to the pairing energy which was evaluated as one-half the mass difference between experimental-mass excess versus Z parabolas of even-mass isotopes in the $A=90$ mass region. The value so obtained gave $\delta=1.3$ MeV. The level density of an odd nuclide was therefore calculated from the true ground state, that of an odd-mass nuclide from a ground state 1.3 MeV above true ground, and that of an even nuclide from a ground state 2.6 MeV above true ground. These pairing corrections were applied to all level-density models used in this work with solely phenomenological justification.[30] Binding energies and pairing energies were both taken from the masses of Mattauch et al., where available.[31] Extrapolated masses were from the mass formula of Myers and Swiatecki.[32]

For the standard Fermi-gas level density and for Rosenzweig's model, a level-spacing parameter $a=A/8.5$ was used; this value was consistent with the value

found and used in prior calculations in the $A=60$ region. Since Eq. (2) cannot reproduce level-density irregularities resulting from shell structure, calculations were also performed using the models of Rosenzweig and Newton.

3. Rosenzweig Level-Density Model

In a level of degeneracy g with n particles and $(g-n)$ holes, there are $g!/[n!(g-n)!]$ ways the particles and holes can be permuted in the ground state without the expenditure of any energy. Margenau[33] suggested that this effect should persist to energies above the ground state. Consequently, closed-shell nuclides at a given excitation would have lower level densities than neighboring nuclides having partially closed shells.

Rosenzweig presented a model yielding a closed-form level-density expression which represents the Margenau effect.[11] Rosenzweig's model assumed that all neutron levels have the same degeneracy g, and all proton levels have the same degeneracy e; all neutron levels were assumed to have equal spacing d_n, and all proton levels to have equal spacing d_p. With this nuclear model, Rosenzweig showed that the Margenau effect could be taken into account explicitly by a displacement ΔE in the ground-state energy of an ordinary Fermi-gas level density, where

$$\Delta E=\tfrac{1}{12}gd_n-(d_n/2g)(n-\tfrac{1}{2}g)^2$$
$$+\tfrac{1}{12}ed_p-(d_p/2e)(p-\tfrac{1}{2}e)^2, \qquad (6)$$

and ΔE is to be added to the thermodynamic excitation energy before calculating $\rho(E)$. In Eq. (6), n and p represent the number of neutrons and protons in the top Fermi level. For the calculations of this work, the level spacings due to Nilsson[34] were used for each nuclide, as well as the actual neutron and proton degeneracies of the highest-filled or partially filled level. Where two levels were very close together, they were assumed to be a single level for purposes of calculating spacing and degeneracy. The actual shifts calculated are shown in Table VII. While the values of ΔE so generated are not truly consistent with Rosenzweig's model, they should give a first approximation to the Margenau effect for the appropriate level densities.

4. Newton Level-Density Model

Since shell effects had been observed experimentally in neutron-capture studies, Newton proposed a modification of the Fermi-gas level density in which shell-model states were used to calculate the variation of single-particle level densities at the Fermi level.[26]

Newton assumed a constant spacing d between shell levels, i.e., groups of $(2j+1)$ coincident or nearly coincident levels for a single particle with spacing d be-

[30] H. Hurwitz and H. Bethe, Phys. Rev. **81**, 898 (1951).

[31] J. H. E. Mattauch, W. Thiele, and A. H. Wapstra, Nucl. Phys. **67**, 1 (1965).

[32] W. D. Myers and W. J. Swiatecki, University of California Lawrence Radiation Laboratory Report No. UCRL-11980, 1965 (unpublished).

[33] H. Margenau, Phys. Rev. **59**, 627 (1941).

[34] S. G. Nilsson, Kgl. Danske Videnskab. Selskab, Mat. Fys. Medd. **29**, No. 16 (1955).

TABLE VII. Energy shifts (MeV) used with Rosenzweig's level-density model.

Mass number (A) :	94	93	92	91	90	89	88	87	86	85
Atomic number (Z)										
42	2.37	1.87	−0.13	1.67	3.07	4.07	4.67	4.87	4.67	
41		0.97	0.47	−1.53	0.27	1.67	2.67	3.27	3.47	3.27
40			0.60	0.10	−1.90	−0.10	1.30	2.30	2.90	3.10
39				1.40	0.90	−1.10	0.70	2.10	3.10	3.70
38					2.28	1.17	0.23	1.50	2.97	3.97
37						2.53	2.03	0.22	1.83	3.23

tween groups. The single-particle levels then have an average density

$$g=d^{-1}(2j+1). \qquad (7)$$

Adopting a spherical nuclear well for the average nuclear potential, Newton showed that $d \propto A^{-2/3}$ and postulated that the level-spacing parameter

$$a=2\alpha A^{2/3}(j_n+j_p+1), \qquad (8)$$

where $a=g_n+g_p$, j_n and j_p are, to first approximation, the spins of the top occupied neutron and proton levels in the nuclear ground state based on Klinkenberg's experimentally determined values,[35] and α is a constant to be evaluated from experimental measurements. Newton actually replaced the spins j_n and j_p of Eq. (5) with "effective spins" $\bar{j}_n$ and $\bar{j}_p$, wherein the spins have been "smoothed" for the effect of nonspherical nuclei away from closed shells and for the number of states about the Fermi level over which the single-particle level densities have been averaged. We have used values of a derived from Eq. (8) with Newton's values of $\bar{j}_n$ and $\bar{j}_p$ and $\alpha=0.0748$ as evaluated by Lang[36] from neutron-capture data. The specific values used are summarized in Table VIII.

V. RESULTS AND DISCUSSION

The experimental excitation functions of this work are compared in Figs. 1(a)–1(f), 1(h) with values calculated using the three level-density models previously discussed. All calculated excitation functions are narrower than the experimentally measured values, with slightly lower thresholds. There may be two phenomena contributing to this situation, one due to γ-ray cascades in the decay process which are not included in the calculation, the other due to contributions from reactions in lighter isotopes (where separated isotope targets were not used). The degree of importance of the latter effect may be seen in Fig. 2, where the calculated excitation functions were computed for the isotopic abundances of the natural targets. The standard Fermi-gas level density was used in these calculations. It would appear that there is a discrepancy in widths beyond that caused by the target's isotopic composition. This broadening has, of course, been observed previously and found to be consistent with what would be expected if the initial compound-nucleus angular momentum were tied up as classical, rigid-body rotational energy with all such rotational energy dissipated in a γ-ray cascade following the emission cascade.[15] This is the so-called s-wave approximation which is discussed in greater detail elsewhere.[15] Several excitation functions calculated with the s-wave approximation and standard Fermi-gas level density are shown in Fig. 3. Generally improved agreement in widths and threshold positions results from use of this model. It has been shown that the s-wave approximation gives quite good agreement with a more rigorous calculation.[10]

TABLE VIII. Level-spacing parameters (MeV⁻¹) used with Newton's level-density model.

Mass number (A) :	94	93	92	91	90	89	88	87	86	85
Atomic number (Z)										
42	13.0	13.5	14.0	14.5	15.0	14.9	14.8	14.7	14.6	
41		10.9	11.4	11.9	12.5	12.7	12.9	12.8	12.6	12.5
49			8.7	9.3	9.8	10.2	10.9	10.8	10.7	10.6
39				7.7	8.2	8.7	9.3	9.8	9.7	9.6
38					8.6	9.1	9.7	10.2	10.7	10.6
37						9.5	10.1	10.6	11.1	11.6

[35] P. F. A. Klinkenberg, Rev. Mod. Phys. 24, 63 (1952).
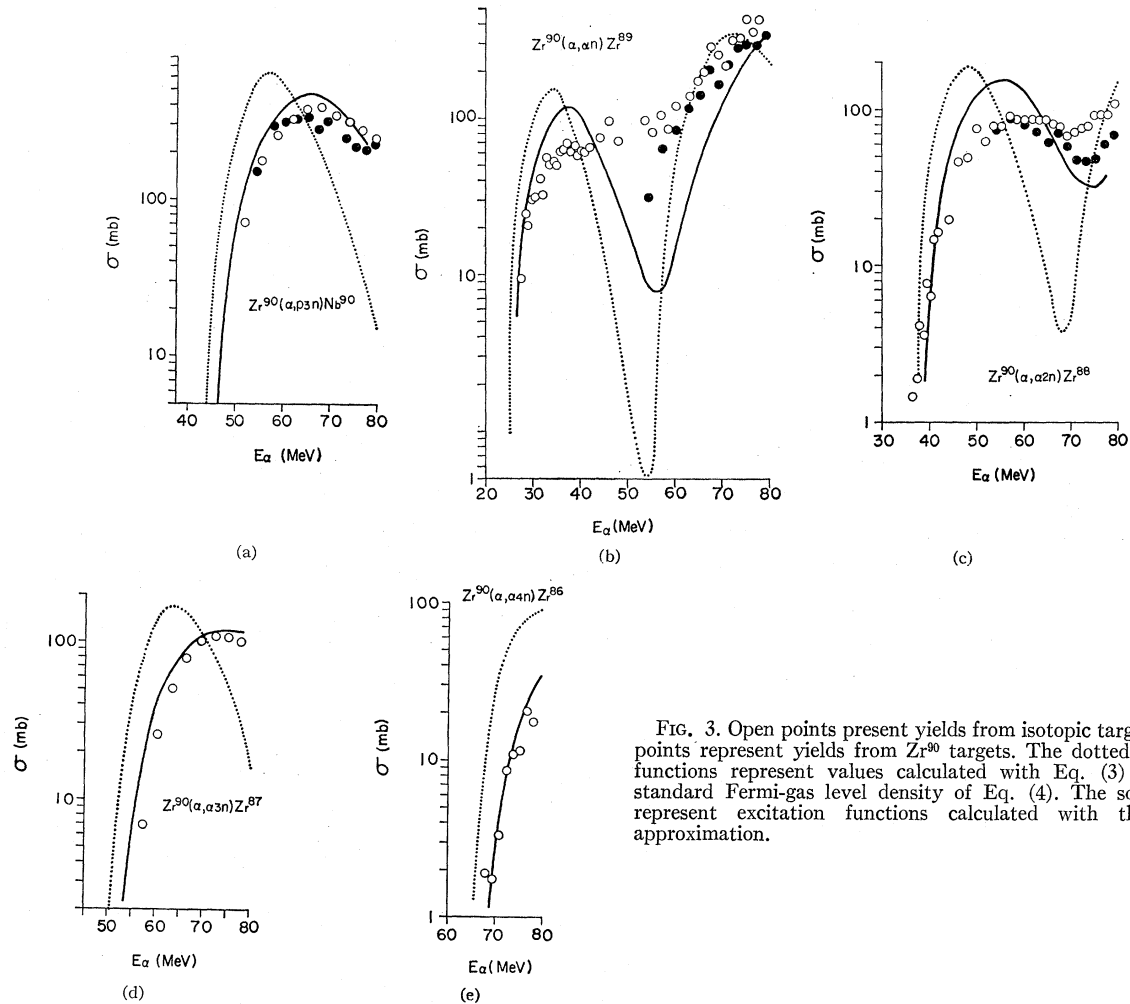[36] D. W. Lang, Nucl. Phys. 26, 434 (1961).

FIG. 3. Open points present yields from isotopic targets; closed points represent yields from Zr⁹⁰ targets. The dotted excitation functions represent values calculated with Eq. (3) using the standard Fermi-gas level density of Eq. (4). The solid curves represent excitation functions calculated with the s-wave approximation.

One purpose of this work, as stated in the Introduction, was to provide data to test the shell-dependent nuclear-level density models. This is done by comparing results calculated with these models with experimental results. Peak yields of excitation functions were selected for these comparisons, rather than making them over the entire excitation functions. This was done because the very rapid variation with energy in the threshold region exaggerates differences in measured and calculated yields where there is a small energy uncertainty. By contrast, there is relatively little energy variation of yields near excitation-function maxima. Additional reasons for making comparisons at excitation-function maxima are the observations from recoil-range data that reaction yields are predominately due to the compound-nucleus mechanism at this point, and the yields are not influenced significantly by contributions from higher-target isotopes where natural targets were used. Where experimental excitation functions show two peaks [e.g., Fig. 3(b)], the comparisons were made on the lower-energy peak.

In Fig. 4, the ratios of calculated to measured yields are shown, at the excitation-function maxima, for the three level-density models previously discussed. The limits on the ratios represent the extremes in the calculated yields due to the two different assumptions on proton versus γ-ray competition below the proton Coulomb barrier. If one of the level-density models were correct, one would expect the ratios of calculated to experimental cross sections to be greater than 1, since the calculated cross section is based on the total nonelastic cross section, which is an upper limit on the compound-nucleus cross section. On the other hand, summing the experimental cross sections at a given energy gives total detected cross sections slightly over one-half the total nonelastic cross section. It follows then that agreement in Fig. 4 means a ratio somewhere between 1 and 2. It would appear that both the standard Fermi-gas level density and the level density modified by Rosenzweig's model give reasonable results.

One method of removing the dependence on compound-nucleus cross sections from these comparisons is

FIG. 4. Comparisons of calculated versus experimental cross sections at excitation-function maxima for the three level-density models indicated. The range of values for each point represents the differences in proton–γ-ray competition assumed, as discussed in the text.
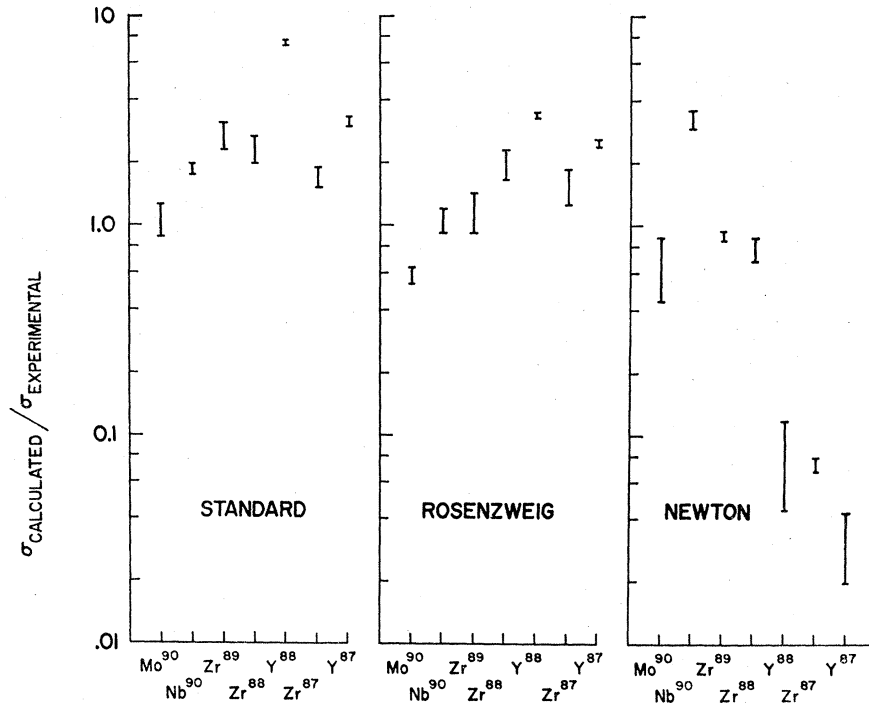
to compare ratios of calculated and experimental isobaric yields. Since the compound-nucleus cross section enters both numerator and denominator in calculating the ratio, it cancels. The ratio of a calculated isobaric-yield ratio to an experimental ratio should, therefore, be unity if the model used for the calculation is correct. Ratios for the isobaric pairs Mo^{90}/Nb^{90}, Zr^{88}/Y^{88}, and Zr^{87}/Y^{87} are shown in Fig. 5. Here the standard level-density formula gives results which differ by an average factor of 2.3 from the experimental ratios; the Rosenzweig model differs by an average factor of 1.7 and Newton's model by an average factor of nearly 8. From these comparisons, it may be seen that the level-
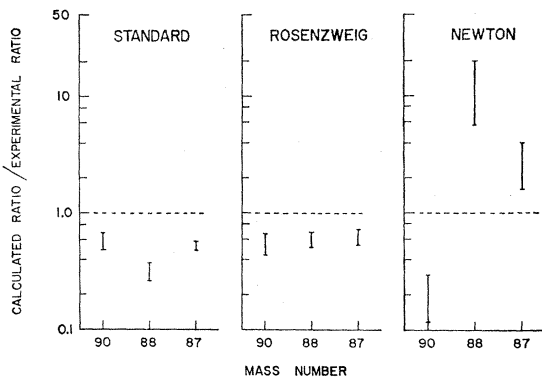

FIG. 5. Ratios of calculated isobaric-yield ratios to experimental isobaric-yield ratios for products of mass number 90, 88, and 87, using three level-density models. The dotted line at 1.0 represents the value which would result if the model were totally valid.

density model of Rosenzweig is satisfactory in interpreting the reactions of this work, as it was in the region of the 28-nucleon shell. The physical differences between the actual level spacings and degeneracies for the nuclides of this work and the idealized model of Rosenzweig make it unreasonable to expect much better agreement. The standard Fermi-gas level-density model is also satisfactory in interpreting these results as it was also satisfactory in the nickel region for those products sufficiently far from the double 28-nucleon shell closure of Ni⁵⁶.

We also conclude that the statistical theory gives a reasonably satisfactory prediction of the energy variation of the excitation functions when provision is made for a γ-ray cascade, as in the case of the s-wave approximation; although it cannot be concluded that the nonequilibrium model of Griffin[13] does not offer an alternative, possibly better, means of interpreting the energy variation. These latter conclusions are highly qualitative and subjective and are best stated by reference to the appropriate figures.

ACKNOWLEDGMENTS